Rotating-radio-frequency ion traps

T. Hasegawa*
Department of Physics, Keio University, Kanagawa 223-8522, Japan

J. J. Bollinger
Time and Frequency Division, National Institute of Standards and Technology, Boulder, Colorado 80305, USA
(Received 9 July 2005; published 20 October 2005)

We discuss a radio-frequency (rf) ion trap, the rotating-radio-frequency (rotating-rf) trap, in which the motion of a charged particle is described by trigonometric functions rather than the usual Mathieu functions of a normal rf trap. In the rotating-rf trap, a rotating quadrupole electric field confines charged particles, whereas in a normal rf trap, an oscillating quadrupole electric field does. Ion motion in a rotating-rf trap is a superposition of two nondegenerate circular secular motions and two corresponding circular micromotions. The cases of applying a uniform dc magnetic field or a quadrupole dc electric field in addition to the rotating-rf field are also discussed. Confinement in a rotating-rf trap can be tighter than in a normal linear rf trap with the same experimental parameter values.

DOI: 10.1103/PhysRevA.72.043403 PACS number(s): 32.80.Pj, 07.75.+h, 52.27.Jt, 82.80.Ms

I. INTRODUCTION

Ion traps are commonly used in many different applications. Examples include quantum-computation studies [1–4], high-resolution spectroscopy and atomic clocks [5–9], nonneutral-plasma physics [10–14], and mass spectroscopy [15,16]. The rf (or Paul) ion trap is particularly useful for applications where a large magnetic field is not desired or important. In atomic physics and quantum optics, for example, rf traps have been used to make careful studies of the interaction of atoms with light [17–19].

The rf trap, which is the three-dimensional version of a magnetic-field-free mass spectrometer invented by Paul in the 1950s [15], uses the force generated by an inhomogeneous, oscillating rf electric field to confine charged particles [20]. A rotating-saddle potential has been used to explain the operation of a rf trap [21]. However, the rotating-saddle trap is not an accurate mechanical analog of the rf trap, because in the case of a rf trap the electric saddle-shaped potential oscillates or "flaps" with the rf drive frequency, whereas in the case of a rotating-saddle trap the gravitational saddle-shaped potential rotates around an axis of gravity [22]. It turns out that motion of a ball in a rotating-saddle trap can be described by trigonometric functions [22], in contrast to those in a rf trap, which are described by Mathieu functions [15,23,24]. Therefore, it is naturally imagined that the motion of a charged particle in an electric version of the rotating-saddle trap could also be described by trigonometric functions and can be simpler than that in a normal rf trap. Simpler ion motion could be useful for some of the applications and studies that use rf traps.

In this paper we discuss a trapping scheme that is an electric version of the rotating-saddle trap. The trap consists of a dc electric field for the confinement in one direction (z) and a rotating quadrupole electric field for confinement in the orthogonal (radial) directions. The rotating-rf (rrf) trap is similar to the commonly used linear rf (lrf) trap [5]. The difference is that the oscillating rf quadrupole electric field in the lrf trap is replaced by a rotating rf quadrupole field in the rrf trap. The rotating quadrupole electric field can be generated by applying sinusoidal voltages with different phases to six or more electrodes that azimuthally surround the trap. This method has been used to generate a rotating electric field in a Penning trap in order to control the plasma rotation frequency, a method sometimes referred to as a rotating wall [25,26].

II. STABILITY OF ROTATING-rf TRAPS

A rrf trap consists of a static electric potential (Φ_z) for axial confinement and a rotating electric potential (Φ_r) for radial confinement. These are expressed as

$$\Phi_z = -\frac{V_d}{r_d^2}(r^2 - 2z^2),$$

$$\Phi_r = \frac{V_r}{r_r^2} r^2 \cos[2(\theta + \omega t)]. \tag{1}$$

Here, r, θ, and z describe the position of the particle in cylindrical coordinates, V_d and V_r are the dc and the rotating voltages, r_d and r_r are effective dimensions (including geometric factors) of the electrodes, and ω is the rotation frequency of the field. Positive ω corresponds to rotation in the $-\hat{\theta}$ direction, and throughout the rest of this paper we implicitly assume $\omega > 0$. The potentials of Eq. (1) can be provided by electrodes shown in Fig. 1, for example. In Fig. 1, a sinusoidal voltage with a specific phase is applied to each of six rod electrodes. The angular frequency of this voltage is 2ω. The field generated by the configuration of Fig. 1 may contain not only the quadrupole field rotating with frequency ω but also the octupole field rotating with frequency $-\omega$, and higher-order fields. At the center of the trap, however, the

*Electronic address: hasegawa@phys.keio.ac.jp

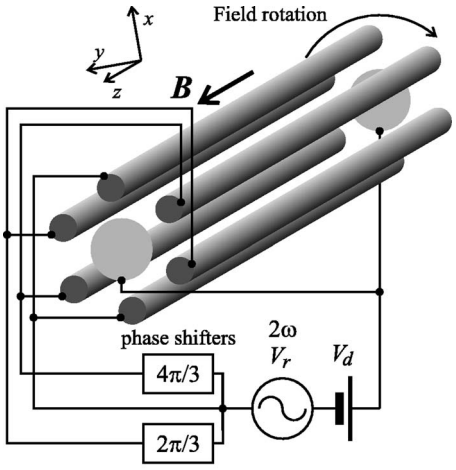

FIG. 1. A possible experimental realization of a rrf trap. The phase shifters delay the ac voltage by the shown phase; namely, if the input of the $2\pi/3$ phase shifter is $V\cos 2\omega t$, the output is $V\cos(2\omega t-2\pi/3)$.

contribution of the quadrupole field is dominant because the spatial dependence of the octupole field is proportional to r^4. In addition to the fields of Eq. (1), we also consider a uniform magnetic field B pointing in the z direction.

The equations of motion can be written as

$$\frac{d^2x}{d\tau^2} = \mu\frac{dy}{d\tau} + dx - 2q(x\cos 2\tau - y\sin 2\tau), \tag{2}$$

$$\frac{d^2y}{d\tau^2} = -\mu\frac{dx}{d\tau} + dy + 2q(x\sin 2\tau + y\cos 2\tau), \tag{3}$$

$$\frac{d^2z}{d\tau^2} = -2dz. \tag{4}$$

Here, $\tau=\omega t$, $\mu\omega=\Omega=eB/m$ is the cyclotron frequency, $d=2eV_d/mr_d^2\omega^2$, $q=eV_r/mr_r^2\omega^2$, and m and e are the mass and charge of the particle, respectively. τ, μ, d, and q are dimensionless. Axial confinement with axial frequency $\omega_z=\sqrt{2d}\omega$ is obtained by choosing positive d. Hence we need to discuss the criteria for stable confinement in only the radial direction. The value of q can be either positive or negative, but physically the sign of q depends only on how the x and y axes are chosen. Therefore, the sign of q will not affect the trap stability.

Throughout this paper we will compare the rrf trap with the lrf trap. We consider a lrf trap whose static electric potential is identical to Φ_z in Eq. (1) and whose rf "flapping" potential is given by

$$\Phi_{\rm lrf} = \frac{V_r}{r_r^2}r^2\cos(2\theta)\cos(2\omega t). \tag{5}$$

This potential can be generated by a standard four-rod trap configuration whose dimensions and rf voltage amplitude are the same as the rrf trap discussed above. The equations of motion for the lrf trap are the same as Eqs. (2)–(4), except that the $2qy\sin 2\tau$ term in Eq. (2) and the $2qx\sin 2\tau$ term in Eq. (3) are missing.

As discussed in Ref. [27], Eqs. (2) and (3) can be solved analytically (with no approximations) by introducing new coordinates (ξ,ζ) in a frame rotating with frequency ω, defined by

$$x = \xi\cos\tau + \zeta\sin\tau,$$

$$y = \zeta\cos\tau - \xi\sin\tau. \tag{6}$$

The solution in the rotating frame is

$$\xi = \sum_{j=1}^{2}(C_je^{i\lambda_j\tau} + D_je^{-i\lambda_j\tau}),$$

$$\zeta = \sum_{j=1}^{2} i\frac{\lambda_j^2 - \mu + d + 1 - 2q}{\lambda_j(\mu-2)}(C_je^{i\lambda_j\tau} - D_je^{-i\lambda_j\tau}), \tag{7}$$

where C_j and D_j are constants determined by the initial conditions, and the λ_j are given by

$$\lambda_1 = \left[\mu - d - 1 + \tfrac{1}{2}(\mu-2)^2 + \tfrac{1}{2}\sqrt{(\mu-2)^2(\mu^2-4d)+16q^2}\right]^{1/2}$$

$$\lambda_2 = \left[\mu - d - 1 + \tfrac{1}{2}(\mu-2)^2 - \tfrac{1}{2}\sqrt{(\mu-2)^2(\mu^2-4d)+16q^2}\right]^{1/2}. \tag{8}$$

If the λ_j have a nonzero imaginary part, the solutions of Eq. (7) diverge exponentially and the trap is not stable. If the λ_j are real valued numbers, the trap is stable. The conditions that must be satisfied simultaneously for real λ_j are

$$(\mu-2)^2(\mu^2-4d)+16q^2 > 0,$$

$$\mu - d - 1 + \tfrac{1}{2}(\mu-2)^2 - \tfrac{1}{2}\sqrt{(\mu-2)^2(\mu^2-4d)+16q^2} > 0. \tag{9}$$

Because ξ is a real variable, C_j and D_j must be complex conjugates of each other for real-valued λ_j. This condition automatically makes ζ real valued. In this case, the solutions in the laboratory frame become

$$x = \sum_{j=1,2}[(1-\gamma_j)A_j\cos(\omega_{j+}\tau + \phi_j) + (1+\gamma_j)A_j\cos(\omega_{j-}\tau - \phi_j)],$$

$$y = \sum_{j=1,2}[(1-\gamma_j)A_j\sin(\omega_{j+}\tau + \phi_j) + (1+\gamma_j)A_j\sin(\omega_{j-}\tau - \phi_j)], \tag{10}$$

where $A_je^{i\phi_j}=C_j=D_j^*$, $\gamma_j=(\lambda_j^2-\mu+d+1-2q)/[\lambda_j(\mu-2)]$, and $\omega_{j\pm}=-1\pm\lambda_j$ $(j=1,2)$ are the normalized characteristic frequencies of the trapped particle motion in the laboratory frame. We note that $\omega_{j-}=-2-\omega_{j+}$. Equation (10) shows that the characteristic motions are circular, and their rotation directions are determined by the sign of the eigenfrequencies.

For the case of a rrf trap, $\mu=0$ (no magnetic field), and the stability condition of Eq. (9) becomes

$$d < q^2,$$

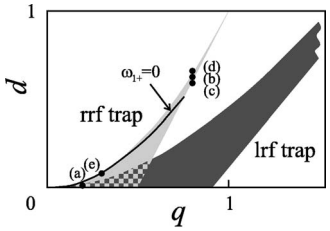

FIG. 2. Stability diagrams in the q-d plane for $\mu=0$ of a rrf and a lrf trap. The stability region of the lrf trap extends to larger q and d, but becomes more narrow as q and d increase. The checked area is the stable region for both traps. Black dots shown correspond to the values of parameters used in Fig. 3. The line shows the parameter values for which one of the secular frequencies (ω_{1+}) becomes zero.

$$d > 2|q| - 1,$$

$$d < 1. \tag{11}$$

Additionally, the condition of $d>0$ is necessary for stability in the z direction. The stability diagram of a rrf trap is shown and compared with the low-order stability region of a lrf trap in Fig. 2 [28]. There is only one stability region for a rrf trap, and its area is smaller than the area of the stability region for the lrf trap.

With $\mu=0$, the eigenfrequencies of Eq. (8) become:

$$\lambda_1 = (1 - d + 2\sqrt{q^2 - d})^{1/2},$$

$$\lambda_2 = (1 - d - 2\sqrt{q^2 - d})^{1/2}, \tag{12}$$

and in the laboratory frame,

$$\omega_{1\pm} = -1 \pm (1 - d + 2\sqrt{q^2 - d})^{1/2},$$

$$\omega_{2\pm} = -1 \pm (1 - d - 2\sqrt{q^2 - d})^{1/2}. \tag{13}$$

ω_{1-} and $\omega_{2\pm}$ are always negative, corresponding to circular motion in the $-\hat{\theta}$ direction (the same direction as the applied rotating potential). ω_{1+} can be of either sign, but is positive (corresponding to circular motion in a direction opposite to the applied rotating potential) for a trap with weak axial confinement ($d \ll q$). Therefore in general the radial motion is composed of circular components rotating in both directions. For the special case $d=-2+2\sqrt{1+q^2}$, which is shown in Fig. 2, ω_{1+} is zero, and the terms associated with ω_{1+} in the solutions of Eq. (10) are constants [$x=(1-\gamma_1)A_1 \cos\phi_1$ and $y=(1-\gamma_1)A_1 \sin\phi_1$].

One advantage of a rrf trap is that there are only four Fourier components in the radial motion, whereas in a lrf trap the radial motion, which is described by Mathieu functions, has an infinite number of Fourier components ($n\Omega_{\rm rf} \pm \omega_{\rm secular}$, where $\Omega_{\rm rf}$ is the applied rf frequency, $\omega_{\rm secular}$ is the secular frequency, and n is any integer). This could mean for example that the optical spectral lines of energetic ions in the rrf trap can be simpler than those in the lrf trap because of fewer motional sidebands.

Some examples of trajectories of a particle are shown in Fig. 3. The trajectories were calculated by numerical integration using the fourth-order Runge-Kutta method, although the analytical solutions [Eqs. (6) and (7)] could also have been used. A large-radius secular motion with a small circular micromotion, similar to that for a particle in a lrf trap, can be seen, especially in Fig. 3(a). In Fig. 3(e) we set $d=-2+2\sqrt{1+q^2}$, in which $\omega_{1+}=0$ and the corresponding motion is displaced from the center of the trap.

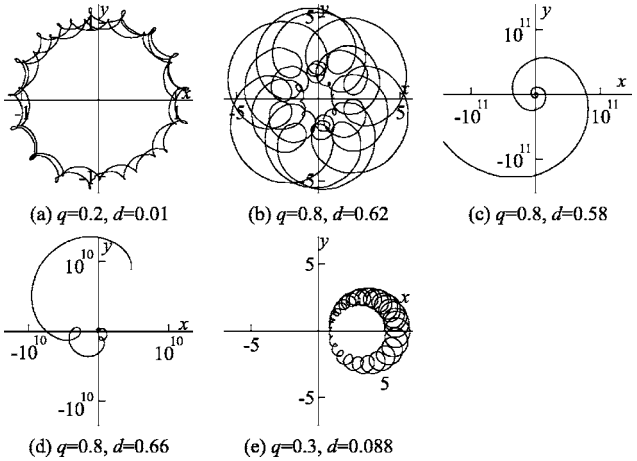

FIG. 3. Examples of trajectories in a rrf trap in the laboratory frame. These trajectories are numerically calculated from $\tau=0$ to 100 by the fourth-order Runge-Kutta method with $x=1$, $y=0$, $dx/d\tau=0$, and $dy/d\tau=0$ as initial conditions. The particle is trapped in (a), (b), and (e), whereas it is unstable in (c) and (d). The values of the q and d parameters are shown in Fig. 2. Especially in (a), a large circular secular motion with a small micromotion can be seen. For (e), the parameter values are chosen so that $\omega_{1+}=0$, in which case the ω_{1+} secular motion is just a displacement from the trap center.

III. PARTICLE MOTION IN A ROTATING-rf TRAP

In this section we discuss the motion of a charged particle in a rrf trap for weak drive amplitude corresponding to $q^2 \ll 1$. Although we have obtained the exact solutions for a rrf trap, this approximate analysis will help us to understand the dynamics. In a lrf trap, a pseudopotential approximation works well in this regime. That is, for time scales that are long compared to the period of the rf drive, the confining force due to the inhomogeneous rf fields can be derived from a potential called the pseudopotential. For the lrf trap the pseudopotential is cylindrically symmetric and characterized by a frequency $\omega_{\rm lrf}$ called the secular frequency. For $q^2 \ll 1$ the lrf trap secular frequency is given by $\omega_{\rm lrf} \sim \sqrt{q^2/2 - d} \ll 1$. The general motion is a superposition of this slow secular motion and rapid micromotion at multiples of the rf drive frequency (−2 in normalized units).

To second order in q and $\sqrt{q^2-d}$, and to first order in d, the characteristic frequencies of Eq. (13) are given by

$$\omega_{1+} \sim \sqrt{q^2 - d} - \frac{q^2}{2},$$

$$\omega_{2+} \sim -\sqrt{q^2 - d} - \frac{q^2}{2},$$

$$\omega_{1-} \sim -2 - \sqrt{q^2 - d} + \frac{q^2}{2},$$

$$\omega_{2-} \sim -2 + \sqrt{q^2 - d} + \frac{q^2}{2}. \tag{14}$$

Expanding the γ_j's to first order in small parameters, the laboratory-frame solutions of Eq. (10) become

$$x \sim \sum_{j=1,2} [(2-q)A_j \cos(\omega_{j+}\tau + \phi_j) + qA_j \cos(\omega_{j-}\tau - \phi_j)],$$

$$y \sim \sum_{j=1,2} [(2-q)A_j \sin(\omega_{j+}\tau + \phi_j) + qA_j \sin(\omega_{j-}\tau - \phi_j)]. \tag{15}$$

We see that ω_{1+} and ω_{2+} are the frequencies of two, in general nondegenerate, circular secular motions. $\omega_{1-}=-2-\omega_{1+}$ and $\omega_{2-}=-2-\omega_{2+}$ are almost equal to the driving frequency [-2 in the normalized units of Eqs. (2)–(4)]. Therefore they are the frequencies of two circular micromotions. The radius of the micromotion is $\sim q/2$ times smaller than the radius of the secular motion.

Equation (14) shows that to first order the secular frequencies are $\pm\sqrt{q^2-d}$. Therefore in this lowest-order approximation, the two secular motions are degenerate, corresponding to circular motions of the same frequency but opposite directions. This is similar to the lrf trap, except the secular frequency in the rrf trap is $\sqrt{2}$ larger for the same q (i.e., the same amplitude and frequency of the applied ac field). However, in the rrf trap, the degeneracy of the secular frequencies is broken in second order. This is to be contrasted with the lrf trap, where the secular frequencies for the x and y motion are degenerate to all orders of q and d.

The breaking of the degeneracy of the secular frequencies produces a precession in the motion of a charged particle in a rrf trap at a frequency $-q^2/2$. In Eq. (15) let $x=X+x_m$ and $y=Y+y_m$, where X and Y represent the secular motion (the ω_{j+} terms) and x_m and y_m represent the micromotion (the ω_{j-} terms). Consider the secular motion only and, as an example, assume an initial ($\tau=0$) position and velocity of the particle's secular motion of $X=1$, $Y=0$, $\dot{X}=0$, and $\dot{Y}=0$. Keeping second-order contributions to the characteristic frequencies but only first-order contributions to the amplitudes, we obtain

$$X + iY = e^{-i(q^2/2)\tau}\left(\cos\sqrt{q^2-d}\,\tau + i\frac{q^2}{2\sqrt{q^2-d}}\sin\sqrt{q^2-d}\,\tau\right) \tag{16}$$

for the secular motion of the particle. Equation (16) describes an elliptical particle orbit with aspect ratio of $q^2/(2\sqrt{q^2-d})$ that precesses about the z axis at a frequency $q^2/2$ in the $-\hat{\theta}$ direction.

The precession can also be observed through numerical simulation of Eqs. (2) and (3). Figure 4 shows particle orbits calculated with the fourth-order Runge-Kutta method for $q=0.2$ and different values of d. The initial conditions $x=1$, $y=0$, $\dot{x}=0$, and $\dot{y}=-q$ for the total particle motion (secular plus micromotion) give approximately the same initial conditions for the secular motion used to derive Eq. (16). From $\tau=0$ to 100 the particle orbit precesses approximately 120° ($\sim$2.1 rad), which agrees with the theoretical prediction of $(q^2/2)\tau=2$ radians.

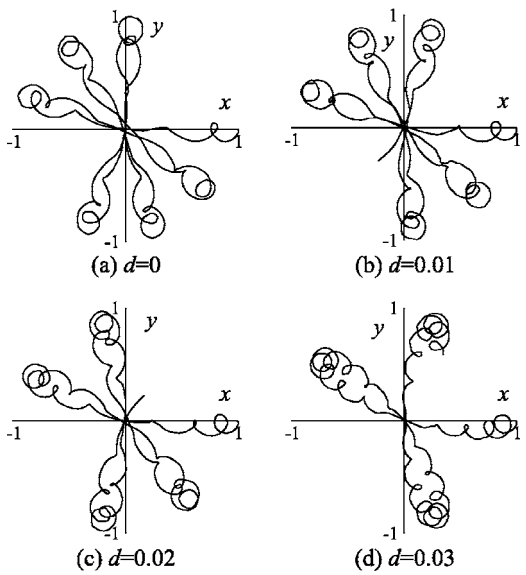

FIG. 4. Precessing secular motions with circular micromotion from $\tau=0$ to 100 when $q=0.2$. Initial conditions are $x=1$, $y=0$, $dx/d\tau=0$, and $dy/d\tau=-q$. In every case, the secular motion precesses about 120° for $\tau=100$, regardless of the value of d.

The breaking of the degeneracy of the secular frequencies is due to different radii of the micromotion associated with the two different secular motions. This can be directly observed by calculating the coefficients $1+\gamma_j$ in Eq. (10) to second order in q. Physically these two secular motions are not equivalent because they correspond to different motions relative to the rotating quadrupole field. The ω_{2+} secular motion corresponds to a circular motion about the trap axis in the $-\hat{\theta}$ direction; that is, a circular motion in the same direction as the rotating field. For an axially weak trap ($d \ll q$) the ω_{1+} secular motion corresponds to a circular motion that opposes the rotating field.

For an axially weak trap ($d \ll q$) and a weak rf drive ($q^2 \ll 1$), we can readily show that the Coriolis force is principally responsible for the difference in the radii of the two micromotions. Consider the case where only the ω_{1+} secular motion is excited [$A_1 \neq 0$ and $A_2=0$ in Eq. (10)] and transform to a frame rotating with ω_{1+}. In this frame the quadrupole potential rotates about the z axis at frequency $-1-\omega_{1+}$. Because this is a quadrupole potential, the electric field at the particle position rotates at a frequency $-2-2\omega_{1+}$. This rotating electric field drives a circular motion at this same frequency. The centrifugal potential in the ω_{1+} rotating frame is $\sim q^2$ and can be neglected for a weak rf drive. Therefore, as sketched in Fig. 5, the particle motion consists principally of circular motion at the frequency $-2-2\omega_{1+}$. The radius ρ_1 of the micromotion is determined by two forces: the force F_{E1} due to the rotating field and the Coriolis force F_{C1} due to the transformation to the ω_{1+} rotating frame. These normalized forces are given by

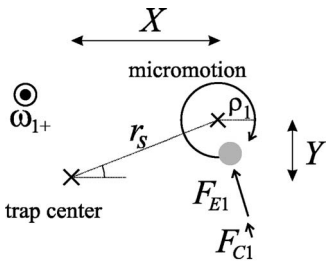

FIG. 5. Schematic representation of the motion of a particle in the frame rotating at ω_{1+} and the forces acting on the particle. F_{E1} and F_{C1} are, respectively, the electric field force and the Coriolis force.

$$F_{E1} = -2qr_s,$$

$$F_{C1} = 2\omega_{1+}(-2-2\omega_{1+})\rho_1 \sim -4\omega_{1+}\rho_1. \tag{17}$$

Here r_s is the cylindrical radius of the center of the micromotion, and negative force means that it points toward the center of the micromotion. For circular motion with radius ρ_1 we must have the relation $F_{E1}+F_{C1}=-(-2-2\omega_{1+})^2\rho_1 \sim -4(1+2\omega_{1+})\rho_1$. From this force balance we obtain

$$\rho_1 = \frac{qr_s}{2(1+\omega_{1+})} \sim \frac{qr_s}{2}(1-\omega_{1+}). \tag{18}$$

This shows that due to the Coriolis force the radius of the micromotion depends on the secular frequency. For the ω_{1+} secular motion, ρ_1 is reduced by ω_{1+}. However, because the ω_{2+} secular motion rotates in the opposite direction ($\omega_{2+}<0$), ρ_2, the micromotion radius for the ω_{2+} secular motion, is increased by $|\omega_{2+}|$. A larger micromotion radius produces a larger secular restoring force. For example, in the laboratory frame and within the approximations of Eq. (18) we can write the ω_{1+} secular and corresponding micromotion as

$$x+iy = X+iY+\frac{q(1-\omega_{1+})}{2}(X-iY)e^{-2i\tau}. \tag{19}$$

By substituting Eq. (19) into Eqs. (2) and (3) and collecting slowly varying terms we obtain

$$\frac{d^2}{d\tau^2}(X+iY) = [d-q^2(1-\omega_{1+})](X+iY). \tag{20}$$

Because Eq. (20) is the equation for the secular motion, the coefficients of the right-hand side must be $-\omega_{1+}^2$. Therefore we obtain $\omega_{1+} \sim \pm\sqrt{q^2-d-q^2/2}$, and apparently the plus sign should be chosen. Likewise, we obtain the same equation for ω_{2+}, and hence the minus sign is for ω_{2+}. This result agrees with Eq. (14) when $d \ll q$.

IV. MODIFICATIONS OF ROTATING-rf TRAPS

A. Uniform magnetic field

With a uniform magnetic field along the z direction, the radial motion of a particle is still described by four Fourier components as shown in Sec. II. This trap should be referred to as a rrf Penning trap. Stability conditions of a rrf Penning trap were already obtained in Eq. (9) and in Ref. [27]. Figure 6 shows stability diagrams for some values of μ in the q-d plane. For $\mu>1$ and $d=\mu-1$, the trap is unstable regardless of q. In this case ω is either one of two characteristic frequencies of a Penning trap, namely, the magnetron frequency $\left[\omega_m=\frac{1}{2}(\Omega-\sqrt{\Omega^2-2\omega_z^2})\right]$ or modified cyclotron frequency $\left[\Omega_m=\frac{1}{2}(\Omega+\sqrt{\Omega^2-2\omega_z^2})\right]$ [29]. Consequently, this instability is due to parametric excitation of a Penning trap motional frequency by the applied rotating quadrupole electric field. The case of $\omega \sim \omega_m$ was investigated in detail experimentally in Ref. [27].

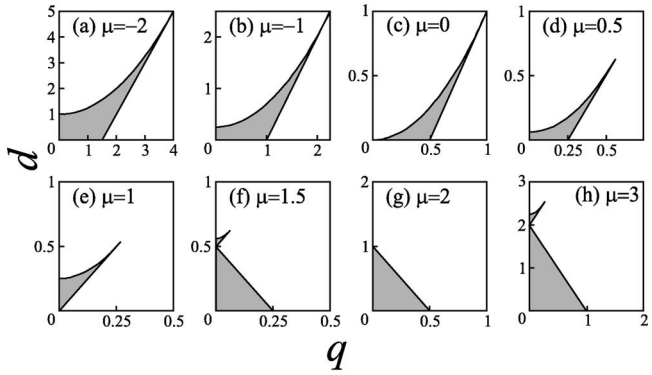

FIG. 6. Stability diagrams in the q-d plane for some specific values of μ. The case of $\mu=0$ (c) is the same as Fig. 2.

The eigenfrequencies in a rrf Penning trap are given by the $\omega_{j\pm}$. [$\omega_{j\pm}=-1\pm\lambda_j$ where the λ_j are given by Eq (8).] For the special case of $q=0$, these become (when $\mu<2$)

$$\omega_{1+} = -\frac{\mu}{2}+\frac{1}{2}\sqrt{\mu^2-4d},$$

$$\omega_{1-} = -2+\frac{\mu}{2}-\frac{1}{2}\sqrt{\mu^2-4d},$$

$$\omega_{2+} = -\frac{\mu}{2}-\frac{1}{2}\sqrt{\mu^2-4d},$$

$$\omega_{2-} = -2+\frac{\mu}{2}+\frac{1}{2}\sqrt{\mu^2-4d}. \tag{21}$$

Hence ω_{1+} is the magnetron frequency (normalized units), and ω_{2+} is the modified cyclotron frequency in a Penning trap. There is no motion corresponding to ω_{1-} or ω_{2-}, because the amplitudes of these motions, $1+\gamma_j$ [Eq. (10)], are zero if $q=0$. For the case of $\mu>2$, ω_{1-} is a modified cyclotron frequency, and ω_{2-} is a magnetron frequency.

B. Static quadrupole potential

One of the important applications of rf traps is mass spectroscopy. In particular the lrf trap in the limit $d=0$ is frequently used as a quadrupole mass filter (QMF) [15,16]. For mass spectroscopy a static quadrupole field given by the expression $V_s(x^2-y^2)/r_r^2$ is applied in addition to the oscillating quadrupole field. Mass spectroscopy is typically accom-

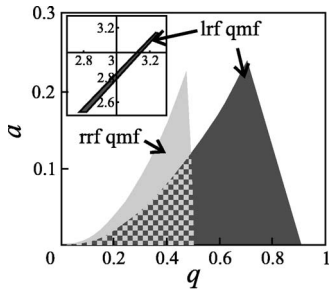

FIG. 7. Stability diagrams of a rrf and a lrf QMF in the q-a plane. The checked area is the stable region for both filters. One of the small stability regions at high q and a of a lrf QMF is also shown as an inset. There is only one stable region for a rrf QMF.

plished by adjusting the rf frequency while keeping the voltages of the static and rf quadrupoles constant to confine charged particles whose charge-to-mass ratio lies within a particular range.

Here we consider the case in which a static quadrupole potential $V_s(x^2-y^2)/r_r^2$ is applied in addition to the rotating rf field of a rrf trap. We consider only the case of $\mu=d=0$. The equations of motion become

$$\frac{d^2x}{d\tau^2} = -2qx\cos 2\tau + 2qy\sin 2\tau - ax,$$

$$\frac{d^2y}{d\tau^2} = 2qy\cos 2\tau + 2qx\sin 2\tau + ay, \tag{22}$$

where a is a dimensionless parameter defined as $2eV_s/mr_r^2\omega^2$.

The transformation of (x,y) to (ξ,ζ) of Eq. (6) no longer simplifies Eq. (22). Therefore, motions in this trap must be expressed by Mathieu-type functions. The solutions can be obtained by an analysis that is a two-dimensional version of that used for Mathieu equations [24]. Details of this analysis are shown in the Appendix.

From the analysis in the Appendix we obtain the stability diagram in the q-a plane of a rrf QMF (Fig. 7). For comparison we also show the stability diagram of an lrf QMF in this figure. In the rrf QMF there are no stability conditions of higher order, in contrast to the lrf QMF, for which additional small stability regions exist (around $a=3$ and $q=3$, for example). The simpler stability diagram of the rrf QMF could have advantages for mass spectroscopy. In addition the range of q in the rrf QMF stability region is lower than that of the lrf QMF. Therefore the rrf QMF can be operated with smaller values of q. This may also provide some advantages for mass spectroscopy; for example, the upper limit of the mass range of a rrf QMF can be higher than that of a lrf QMF, since q is proportional to $1/m$.

V. CONCLUSIONS

We have discussed a proposal for a rotating-rf trap, in which the ion motion is described by simple trigonometric functions. This simple ion motion might be advantageous, for example, in producing simpler motional sidebands of optical spectral lines of trapped ions compared to those in a lrf trap. The simplicity of the classical motion in a rrf trap may also simplify the quantum-mechanical analysis of this trap. As far as we know, the rrf trap is the only type of rf trap that is not expressed by a Mathieu-type solution. The motion of a particle in a rrf trap is composed of two circular secular motions and two corresponding circular micromotions. For an axially weak trap ($d \ll q$) one of the secular motions rotates in a direction opposite to that of the rotating field, and the other secular motion rotates in the same direction. The difference in the absolute values of the secular frequencies is of order q^2, and this difference causes a precession of the secular motion. The secular frequency in a rrf trap is $\sqrt{2}$ larger than that for a lrf trap with the same trap parameters. Therefore tighter confinement can be achieved in a rrf trap.

If a uniform magnetic field is applied along the trap axis the motion is still described by trigonometric functions. However, applying a static quadrupole electric field requires Mathieu-like functions to describe the ion motion. The stability diagram of a rrf quadrupole mass filter with static quadrupole field was obtained. The rrf QMF may have some advantages over lrf QMF's due to its single stability region, which occurs for lower values of q.

ACKNOWLEDGMENTS

This research was partially supported by the Japan Society for the Promotion of Science, Grant-in-Aid for Scientific Research No. 16740232. We thank W. Oskay (NIST) and M. Jensen (NIST) for their comments on the manuscript.

APPENDIX: STABILITY CONDITIONS OF TWO-DIMENSIONAL MATHIEU EQUATION

The differential equations to be solved here are given by Eq. (22). By Floquet's theorem the solutions can be expressed as

$$x = \sum_{j=1,2} [A_j e^{\beta_j \tau}\psi_j(\tau) + B_j e^{-\beta_j \tau}\psi_j(-\tau)],$$

$$y = \sum_{j=1,2} [C_j e^{\beta_j \tau}\psi_j(\tau) + D_j e^{-\beta_j \tau}\psi_j(-\tau)]. \tag{A1}$$

Here, $\psi_j(\tau)$ is a function of τ with a period of π, namely, $\psi_j(\tau+\pi)=\psi_j(\tau)$, and A_j, B_j, C_j, and D_j are constants determined by initial conditions. There are eight constants, which may seem like too many, but four of them are functions of the others.

The factor β_j is determined by q and a. Because of the periodicity of ψ_j, the imaginary part of β_j is arbitrary up to a multiple of $2i$, $\beta_j=\beta_{j,p}+2in$ (n is an integer, and $\beta_{j,p}$ is a principal value). Further, the sign of β_j is arbitrary, because both of $e^{\beta_j\tau}$ and $e^{-\beta_j\tau}$ appear in Eq. (A1). For convenience, we choose $0 \leqslant \mathrm{Im}(\beta_j) \leqslant 1$ as the principal value. To determine β_j and $\psi_j(\tau)$, the second terms of the right-hand side of Eq. (A1) are not necessary, and hereafter we suppose $B_j = D_j = 0$.

Because of the periodicity, $\psi_j(\tau)$ can be expanded as

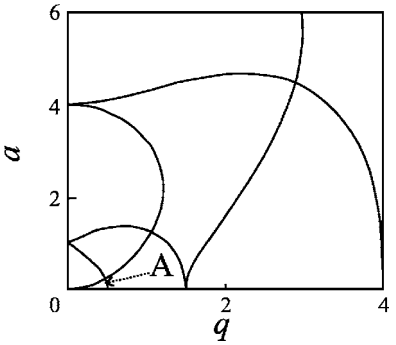

FIG. 8. Lines of $\beta=0$ and $\beta=i$ for the solutions of a rrf QMF in the q-a plane. The region labeled A is the only stable region.

$$\psi_j(\tau) = \sum_{k=-\infty}^{\infty} c_{j,k} e^{2ik\tau}. \tag{A2}$$

By substituting Eqs. (A1) and (A2) into Eq. (22) and equating terms of the same frequencies, we have

$$\begin{aligned}[(\beta_j + 2ik)^2 + a]A_j c_{j,k} &= -q(A_j c_{j,k-1} + A_j c_{j,k+1}) \\ &\quad - iq(C_j c_{j,k-1} - C_j c_{j,k+1}),\end{aligned}$$

$$\begin{aligned}[(\beta_j + 2ik)^2 - a]C_j c_{j,k} &= -iq(A_j c_{j,k-1} - A_j c_{j,k+1}) \\ &\quad + q(C_j c_{j,k-1} + C_j c_{j,k+1}).\end{aligned} \tag{A3}$$

A necessary and sufficient condition for the existence of a nontrivial solution of Eq. (A3) is

$$\Delta_j(\beta_j) = 0, \tag{A4}$$

where

$$\Delta_j(\beta_j) = \begin{vmatrix} \ddots & \ddots & 0 & 0 & 0 \\ \ddots & I & Q^{(-)}_{j,k-1} & 0 & 0 \\ 0 & Q^{(+)}_{j,k} & I & Q^{(-)}_{j,k} & 0 \\ 0 & 0 & Q^{(+)}_{j,k+1} & I & \ddots \\ 0 & 0 & 0 & \ddots & \ddots \end{vmatrix}, \tag{A5}$$

$$Q^{(\pm)}_{j,k} = \begin{pmatrix} \dfrac{q}{(\beta_j - 2ik)^2 + a} & \pm i\dfrac{q}{(\beta_j - 2ik)^2 + a} \\ \pm i\dfrac{q}{(\beta_j - 2ik)^2 - a} & -\dfrac{q}{(\beta_j - 2ik)^2 - a} \end{pmatrix}, \tag{A6}$$

$$I = \begin{pmatrix} 1 & 0 \\ 0 & 1 \end{pmatrix}. \tag{A7}$$

The determinant $\Delta_j(\beta_j)$, which consists of an infinite number of elements, has a period of $2i$ in β_j. Equation (A4) is identical regardless of j, and this suggests that two solutions of Eq. (A4) should be obtained. In fact, it turns out later that this suggestion is correct, and hence we will stop using the subscript j.

The determinant $\Delta(\beta)$ can be obtained as follows. $\Delta(\beta)$ has poles at $\beta = 2ik \pm \sqrt{\pm a}$. A function $\chi(\beta)$ defined as

$$\chi(\beta) = \frac{\cos(i\pi\beta) + \epsilon}{[\cos(i\pi\beta) - \cos(i\pi\sqrt{a})][\cos(i\pi\beta) - \cos(i\pi\sqrt{-a})]} \tag{A8}$$

also has the same poles (ϵ is a constant determined later). Therefore, $\Delta(\beta) - \kappa\chi(\beta)$ has no singularities if κ and ϵ are chosen suitably and must be a constant by Liouville's theorem. The constants κ and ϵ can be determined as follows. When $\mathrm{Re}(\beta) \to \infty$, all off-diagonal elements of Eq. (A5) tend to zero, and hence

$$\lim_{\mathrm{Re}(\beta)\to\infty} \Delta(\beta) = 1, \tag{A9}$$

and from Eq. (A8),

$$\lim_{\mathrm{Re}(\beta)\to\infty} \chi(\beta) = 0. \tag{A10}$$

Then we have for any β,

$$\Delta(\beta) - \kappa\chi(\beta) = 1. \tag{A11}$$

When $|\beta| \ll 1$, $\chi(\beta)$ is expanded as

$$\begin{aligned}\chi(\beta) &= \frac{1 + \epsilon}{(1 - b_+)(1 - b_-)} + \frac{b_+ b_- - 1 + \epsilon(b_+ + b_- - 2)}{2(1 - b_+)^2(1 - b_-)^2}\pi^2\beta^2 \\ &\quad + O(\beta^4),\end{aligned} \tag{A12}$$

where $b_\pm = \cos(i\pi\sqrt{\pm a})$. On the other hand, $\Delta(\beta)$ is expanded as

$$\Delta(\beta) = \Delta(0) + \frac{1}{2}\frac{d^2\Delta(0)}{d\beta^2}\beta^2 + O(\beta^4). \tag{A13}$$

Note that $\Delta(\beta)$ must be an even function of β [see Eqs. (A8) and (A11)]. From the zeroth- and second-order terms of Eqs. (A12) and (A13) and using Eq. (A11), we have

$$\begin{aligned}\kappa &= \frac{(1 - b_+)(1 - b_-)}{\pi^2}\left(\frac{d^2\Delta(0)}{d\beta^2}(1 - b_+)(1 - b_-)\right. \\ &\quad \left. - \pi^2[\Delta(0) - 1](b_+ b_- - 2)\right)\end{aligned}$$

$$\epsilon = \frac{\pi^2[\Delta(0) - 1](b_+ b_- - 1) - [d^2\Delta(0)/d\beta^2](1 - b_+)(1 - b_-)}{[d^2\Delta(0)/d\beta^2](1 - b_+)(1 - b_-) - \pi^2[\Delta(0) - 1](b_+ b_- - 2)}. \tag{A14}$$

To determine β, which satisfies Eq. (A4), we use Eq. (A11) and obtain

$$\begin{aligned}\beta &= \frac{1}{i\pi}\cos^{-1} \\ &\quad \times\left(\frac{1}{2}[b_+ + b_- - \kappa \pm \sqrt{(b_+ + b_- - \kappa)^2 - 4\kappa\epsilon - 4b_+ b_-}]\right).\end{aligned} \tag{A15}$$

Consequently, β can be obtained by computing $\Delta(0)$ and

$d^2\Delta(0)/d\beta^2$ and by substituting them into Eq. (A15). It is found that there are two solutions of β in Eq. (A15), and as stated before, one of them is β_1 and the other is β_2. As mentioned previously, the sign of β is arbitrary, and this is expressed in Eq. (A15) through the arbitrary sign of the arccosine function.

To compute $\Delta(0)$ and $d^2\Delta(0)/d\beta^2$, we must approximate the infinite-dimensional matrix of Eq. (A5) to that of a finite number of elements. The off-diagonal elements can be approximated as zero except when $k^2 \sim \pm a/4$. Therefore we consider only elements where $k \sim \pm\sqrt{\pm a}/2$. When $a = \pm 4k^2$, it seems at first that we cannot compute $\Delta(0)$ and $d^2\Delta(0)/d\beta^2$ because of the singularity; but we can calculate β in Eq. (A15) by supposing $a \neq \pm 4k^2$ and finally taking the limit of $a \to \pm 4k^2$.

The stability diagram in the q-a plane can be obtained by calculating β as a function of q and a. Stable and unstable regions are separated from each other by the $\beta = 0$ and $\beta = i$ lines, which are shown in Fig. 8. Whether the solution inside each region is stable or unstable can be found by calculating $\mathrm{Re}(\beta)$. If $\mathrm{Re}(\beta) \neq 0$, the solution exponentially diverges. It turns out that the region named A in Fig. 8 is the only stable region, which is the stability region of a rrf QMF shown in Fig. 7.

[1] M. D. Barrett, J. Chiaverini, T. Schaetz, J. Britton, W. M. Itano, J. D. Jost, E. Knill, C. Langer, D. Liebfried, R. Ozeri, and D. J. Wineland, Nature (London) **429**, 737 (2004).

[2] J. I. Cirac and P. Zoller, Phys. Rev. Lett. **74**, 4091 (1995).

[3] J. Pachos and H. Walther, Phys. Rev. Lett. **89**, 187903 (2002).

[4] H. Häffner, S. Gulde, M. Riebe, G. Lancaster, C. Becher, J. Eschner, F. Schmidt-Kaler, and R. Blatt, Phys. Rev. Lett. **90**, 143602 (2003).

[5] J. D. Prestage, G. J. Dick, and L. Maleki, J. Appl. Phys. **66**, 1013 (1989).

[6] J. C. Bergquist, S. R. Jefferts, and D. J. Wineland, Phys. Today **54** (3), 37 (2001).

[7] G. P. Barwood, H. S. Margolis, G. Huang, P. Gill, and H. A. Klein, Phys. Rev. Lett. **93**, 133001 (2004).

[8] A. A. Madej, J. E. Bernard, P. Dube, L. Marmet, and R. S. Windeler, Phys. Rev. A **70**, 012507 (2004)

[9] Chr. Tamm, D. Engelke, and V. Bühner, Phys. Rev. A **61**, 053405 (2000).

[10] D. H. E. Dubin and T. M. O'Neil, Rev. Mod. Phys. **71**, 87 (1999).

[11] W. M. Itano, J. J. Bollinger, J. N. Tan, B. Jelenković, X.-P. Huang, and D. J. Wineland, Science **279**, 686 (1998).

[12] L. Hornekaer and M. Drewsen, Phys. Rev. A **66**, 013412 (2002).

[13] J. Estrada, T. Roach, J. N. Tan, P. Yesley, and G. Gabrielse, Phys. Rev. Lett. **84**, 859 (2000).

[14] P. Paasche, T. Valeuzuela, D. Biswas, C. Angelescu, and G. Werth, Eur. Phys. J. D **18**, 295 (2002).

[15] W. Paul and H. Steinwedel, Z. Naturforsch. A **8**, 448 (1953).

[16] P. K. Ghosh, *Ion Traps* (Clarendon, Oxford, 1997).

[17] D. J. Wineland, W. M. Itano, and J. C. Bergquist, Opt. Lett. **12**, 389 (1987).

[18] F. Diedrich and H. Walther, Phys. Rev. Lett. **58**, 203 (1987).

[19] T. Sauter, W. Neuhauser, R. Blatt, and P. E. Toschek, Phys. Rev. Lett. **57**, 1696 (1986).

[20] W. Paul, Rev. Mod. Phys. **62**, 531 (1990).

[21] W. Paul, in Laser Manipulation of Atoms and Ions, *Proceedings of the International School of Physics* "Enrico Fermi," Course 118, 1991, edited by E. Arimondo, W. D. Phillips, and F. Strumia, (Elsevier, Amsterdam, 1992).

[22] R. I. Thompson, T. J. Harmon, and M. G. Ball, Can. J. Phys. **80**, 1433 (2002).

[23] R. F. Wuerker, H. Shelton, and R. V. Langmuir, J. Appl. Phys. **30**, 342 (1959).

[24] N. W. McLachlan, *Theory and Application of Mathieu Functions* (Clarendon, Oxford, 1947).

[25] X. -P. Huang, F. Anderegg, E. M. Hollmann, C. F. Driscoll, and T. M. O'Neil, Phys. Rev. Lett. **78**, 875 (1997).

[26] X. -P. Huang, J. J. Bollinger, T. B. Mitchell, W. M. Itano, and D. H. E. Dubin, Phys. Plasmas **5**, 1656 (1998).

[27] T. Hasegawa, M. J. Jensen, and J. J. Bollinger, Phys. Rev. A **71**, 023406 (2005).

[28] The stability diagram of a lrf trap with nonzero d is just the stability of a single one-dimensional Mathieu equation, because the equation of motion in x is identical to that in y except for the sign of q, which does not affect the stability.

[29] L. S. Brown and G. Gabrielse, Rev. Mod. Phys. **58**, 233 (1986).